Journal of Materials Chemistry A

COMMUNICATION

View Article Online
View Journal | View Issue

Cite this: J. Mater. Chem. A, 2014, 2, 15303

Received 29th May 2014
Accepted 25th July 2014

DOI: 10.1039/c4ta02690j

www.rsc.org/MaterialsA

High efficiency organic/a-Si hybrid tandem solar cells with complementary light absorption†

Wei Qin,‡[af] Wei Yu,‡[af] Wei Zi,[bc] Xiang Liu,[d] Tao Yuan,[e] Dong Yang,[af] Shubo Wang,[a] Guoli Tu,[e] Jian Zhang,*[a] Frank S. Liu*[abc] and Can Li*[a]

Organic/amorphous silicon (a-Si) hybrid tandem solar cells have the potential to provide a highly efficient low-cost photovoltaic technology using abundant elements, and the technology is adaptable to large-scale processes. With their high open-circuit voltage (V_{oc}) and adaptability to a broad solar spectrum, organic/a-Si tandem devices offer significantly improved performance. We have shown that organic/a-Si hybrid tandem solar cells with a complementary organic absorber can exhibit a power conversion efficiency (PCE) of up to 7.5%, with a fill factor (FF) of 72.3% and a V_{oc} almost equivalent to the sum of the sub-cells under standard air mass (AM) 1.5 illumination. The high performance of the device results from the complementary absorption spectra of two sub-cells and well-matched energy levels of the intermediate layer. This study provides an effective design strategy for organic/a-Si hybrid tandem solar cells of improved efficiency.

Hybrid solar cells have attracted interest due to their ability to combine the advantages of diverse components. Heterojunction and tandem devices are two major structures used in the construction of a hybrid solar cell. A silicon heterojunction with an intrinsic thin layer (HIT) has been applied to achieve world-record efficiency, as high as 24.7%.[1–3] Si-heterojunctions with an organic thin film have also achieved good efficiency, in this case of 11%.[4–6] In the present article, we address the issues in the development of hybrid tandem solar cells.

Solar cells with a single light-absorbing layer are able to utilize only a small fraction of the solar spectrum.[7,8] To make effective use of a broader range of the solar spectrum, tandem devices with as many as four light-absorbing layers have been developed.[8,9] In the first place, tandem devices with materials of multiple bandgap can extend the absorption to cover a broader range of the solar spectrum.[10,11] Secondly, a tandem device gives a higher open circuit voltage (V_{oc}), which can potentially be maximized to be equivalent to the sum of the component cells, V_{oc}s.[11–13] Thirdly, the strategy of employing a wide bandgap material to absorb high energy photons and a narrow bandgap material absorbing longer wavelengths of the spectrum can effectively reduce thermal energy losses, particularly in the case of short-wavelength photons.[8,11,14] Finally, as the V_{oc} is increased and the short-circuit current (J_{sc}) reduced, the spectrum-splitting approach reduces electrical losses within the device, leading to an increased fill factor (FF).[11,15]

During the past decade amorphous-nanocrystalline (a-Si/nc-Si), or micromorphous thin-film, Si tandem solar cells, have gained a great deal of attention due to their low cost and high efficiency.[16–18] The design employs a-Si as the top-cell with bandgap of ~1.7 eV, mainly absorbing in the blue-green section of the solar spectrum.[19,20] Meanwhile a bottom-cell of nc-Si with a narrower bandgap of ~1.1 eV absorbs in the red and near-infrared areas.[21] Unfortunately, as nc-Si is only an indirect bandgap material, a layer several micrometers in thickness is required to efficiently absorb solar light,[20,22,23] increasing the cost of nc-Si solar cells.

Due to the relatively high absorption coefficient of organic semiconductors, a layer of sub-micron thickness is sufficient for absorbing solar light,[24] making them a suitable replacement nc-Si as the bottom-cell absorbers. In addition, organic solar cells (OSCs) can potentially be manufactured using a more cost-effective roll-to-roll printing method,[25,26] significantly reducing the cost of production. Organic/a-Si hybrid tandem solar cells can thus offer high efficiency at a relatively low cost.

[a]State Key Laboratory of Catalysis, Dalian Institute of Chemical Physics, Chinese Academy of Sciences, Dalian National Laboratory for Clean Energy, Dalian 116023, China. E-mail: canli@dicp.ac.cn; jianzhang@dipc.ac.cn; szliu@dipc.ac.cn

[b]Key Laboratory of Applied Surface and Colloid Chemistry, National Ministry of Education, China

[c]School of Materials Science and Engineering, Shaanxi Normal University, Xi'an 710062, China

[d]School of Materials Science and Engineering, Dalian Jiaotong University, Dalian 116023, China

[e]Wuhan National Laboratory for Optoelectronics, Huazhong University of Science and Technology, Wuhan, 430074, China

[f]Graduate University of Chinese Academy of Sciences, Beijing 100049, China

† Electronic supplementary information (ESI) available. See DOI: 10.1039/c4ta02690j

‡ W. Qin and W. Yu contributed equally to this study.

In 2011, Kim *et al.*[27] first reported organic/a-Si tandem solar cells using a conjugated polymer of PCPDTBT (optical bandgap (E_g) = 1.46 eV)[28] to replace nc-Si in micromorph solar cells. However, its relatively low current density and low FF severely limited its cell performance. In 2012 Seo *et al.*[29] reported an organic/a-Si (PBDTTT-C)[30] hybrid tandem solar cell with E_g = 1.61 eV, power conversion efficiency (PCE) of 5.72% and V_{oc} of 1.42 V, by optimizing the intermediate layers. This gave 92% of the sum of the V_{oc} values of the component cells. However, the absorption spectrum of PBDTTT-C overlaps significantly that of a-Si solar cell and absorbs very little light beyond 800 nm. Very recently, Albrecht *et al.* have announced an organic/a-Si double-junction solar cell with PCE > 7%, by optimizing the intermediate layers and using a low bandgap polymer, PCPDTBT.[31] These results show the potential for achieving a high performance hybrid tandem solar cell comprising silicon and an organic polymer. It was therefore vital for us to investigate the key factors influencing performance, such as recombination losses at the intermediate layer between the component cells, and the charge collection ability of the cathode.

In the present study, a narrow bandgap polymer poly(diketopyrrolopyrrole-terthiophene) (PDPP3T), with a bandgap of 1.31 eV, was used as the active layer in OSCs.[32] The UV-vis spectrum of PDPP3T is complementary to that of a-Si solar cells and extends the absorption spectrum of the tandem device to 950 nm. In addition, OSCs have been optimized by the use of a conjugated polyelectrolyte as cathode interface layers (CILs). By applying these approaches, the PCE of optimized organic/a-Si tandem solar cells can attain a value of 7.5%, with FF as high as 72.3%. Meanwhile, the V_{oc} of the hybrid tandem cell can reach 1.51 V, which is almost equal to the sum of the sub-cell V_{oc} values, and is the highest value so far encountered in the lierature.[20,22]

Fig. 1(a) illustrates the structure of an organic/a-Si hybrid double-junction solar cell. The a-Si (p-type/intrinsic/n-type stack) top-cell was deposited on fluorine-doped tin oxide (FTO) glass by radio-frequency plasma-enhanced chemical vapor deposition. The a-Si:H absorbs blue and green light. The bottom-cell (Fig. 1(b)) was constructed from a narrow bandgap conjugated polymer, PDPP3T, blended with [6,6]-phenyl C_{61} butyric acid methyl ester ($PC_{61}BM$), and absorbs red light. The spin-coated PDPP3T:$PC_{61}BM$ layer is ~110 nm thick. The intermediate layer between the a-Si top-cell and the OSC comprises a transparent indium-tin oxide (ITO) layer and a highly conductive poly(3,4-ethylenedioxylenethiophene)-polystyrene sulfonic acid (PEDOT:PSS; Clevios 4083) layer. The ITO was deposited at a thickness of 50 nm on the a-Si top-cell using magnetron sputtering, and the PEDOT:PSS was then spin coated onto the ITO layer at a thickness of ~40 nm. Details are given in the ESI. Fig. 1(c) shows the absorption spectra of PDPP3T:$PC_{61}BM$ and PDPP3T:$PC_{71}BM$ films, along with an a-Si solar cell. In the PDPP3T:$PC_{71}BM$ film, absorption occurred in the range 400–600 nm, unlike its $PC_{61}BM$ counterpart, indicating that the absorption was due to the $PC_{71}BM$ itself. The PDPP3T absorbs mainly in the red and near-infrared regions of the solar spectrum (650–950 nm), whereas the a-Si solar cell shows high transmittance. The spectral response of these two

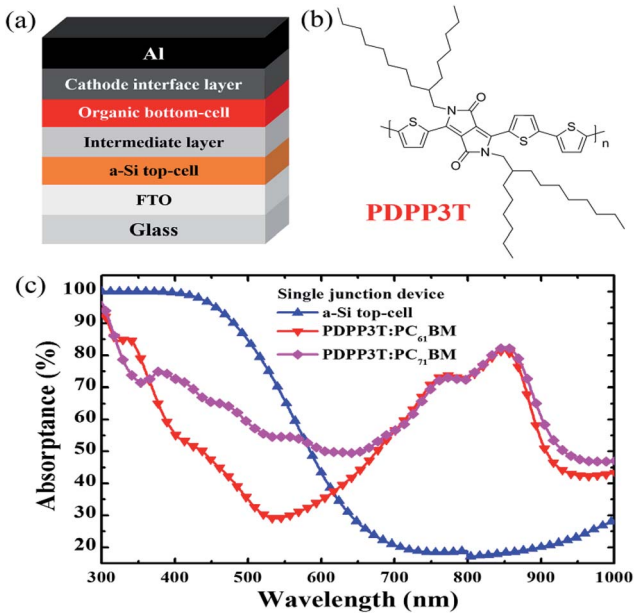

Fig. 1 (a) Structure of an organic/a-Si hybrid tandem solar cell; (b) the chemical structure of the low-bandgap polymer, PDPP3T, used in the hybrid tandem solar cell; and (c) normalized absorption spectra of an organic thin film and a-Si thin film.

systems complements each other satisfactorily, showing the clear advantage of the spectrum-splitting provided by tandem solar cells.

Before being utilized in the hybrid tandem solar cells the single-junction OSCs were optimized. The device structure has the sequence: glass/ITO/PEDOT:PSS/PDPP3T:PCBM/CIL/Al, the PDPP3T:PCBM film being spin-coated from solution in a ternary blend of dichlorobenzene, chloroform and 1,8-diiodooctane (DCB–CF–DIO).[33]

Fig. 2(a) shows the characteristics of a Ca/Al-based OSC used as a control device, under illumination with and without an a-Si top-cell functioning as an optical filter. PDPP3T:$PC_{71}BM$ OSCs exhibit a PCE of 5.60%, whereas in the case of PDPP3T:$PC_{61}BM$ OSCs, the PCE is 5.30%. The performance of PDPP3T:$PC_{71}BM$ OSCs is thus superior to that of PDPP3T:$PC_{61}BM$ OSCs. However, after the incident light has been filtered using an a-Si thin film, as in the hybrid tandem devices, PDPP3T:$PC_{61}BM$ OSCs show superior performance to their PDPP3T:$PC_{71}BM$ counterparts. Using the a-Si filter, PDPP3T:$PC_{71}BM$ OSC gives a J_{sc} of 5.64 mA cm^{-2}, whereas using this filter PDPP3T:$PC_{61}BM$ OSC generates a higher J_{sc}, 5.94 mA cm^{-2}, indicating that $PC_{71}BM$ would not contribute as much current as $PC_{61}BM$ in an organic/a-Si tandem configuration. This result demonstrates that the excess absorption of $PC_{71}BM$ at short wavelengths contributes to the performance of single-junction devices, whereas it makes only a limited contribution to the performance of tandem devices at longer wavelengths.

To further improve the performance of PDPP3T:$PC_{61}BM$ OSCs, an alternative CIL, poly(9,9-bis(4-(sulfonatobutyl)-2,7-fluorene)-*alt*-2,7-(9,9-bis(2-(2-(2-methoxyethoxy)ethoxy)ethyl)-fluorene)) with sodium sulfonate and oligo-(ethylene oxide) side-chains

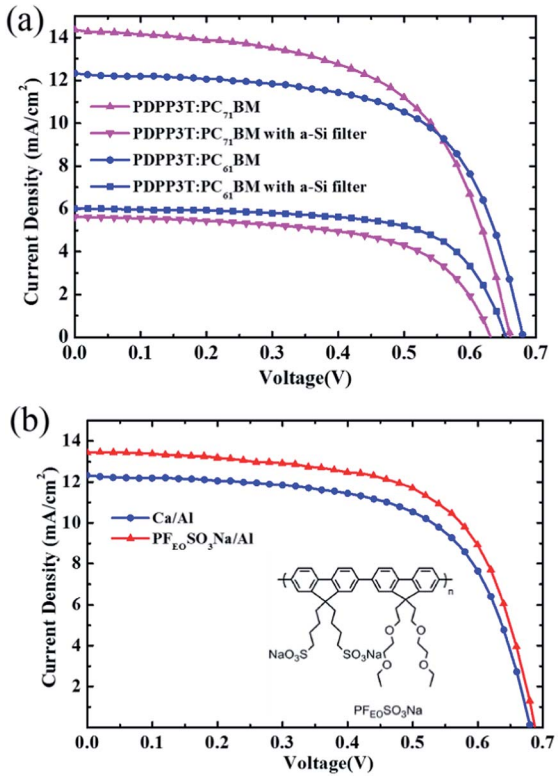

Fig. 2 (a) Current density–voltage (J–V) characteristics of organic single-junction solar cells based on PDPP3T:$PC_{71}BM$ and PDPP3T:$PC_{61}BM$ under illumination of 100 mW cm^{-2}, together with their J–V characteristics under illumination with light filtered using a-Si thin films; (b) J–V characteristics of PDPP3T:$PC_{61}BM$ organic single-junction solar cells with different cathode interface layers.

($PF_{EO}SO_3Na$), was used to replace Ca. Using $PF_{EO}SO_3Na$, a PCE of 5.89% along with J_{sc} of 13.43 mA cm^{-2} was achieved, higher than that obtained with Ca. $PF_{EO}SO_3Na$ can form the desired interfacial dipole at the interface between the active layer and the cathode, and significantly improves the charge collection efficiency in OSCs.[34–36] The J–V characteristics are shown in Fig. 2(b) and the detailed device parameters are summarized in Table 1.

Current matching between the component cells is crucial to achieve good performance in tandem devices. By reducing the thickness of the a-Si top-cell, the optical transmission can be increased to obtain a maximized but balanced photocurrent for the organic bottom-cell. When the thickness of a-Si thin film was decreased from 125 nm to 72 nm, the J_{sc} of the tandem device was markedly increased, from 5.29 mA cm^{-2} to 6.50 mA cm^{-2}, whereas the V_{oc} (1.50 V) and FF (72.3%) were relatively unchanged. The detailed device performance is summarized in Table 2 and the J–V curves are as shown in Fig. S1.† As result, the PCE of the tandem device was increased from 5.75 to 7.06%. A further thinned a-Si top-cell makes the V_{oc} and J_{sc} fall sharply and degrades the performance.

The PCE of the preferred example of a tandem solar cell reaches a value as high as 7.46%, with J_{sc} of 6.73 mA cm^{-2}, V_{oc} of 1.51 V and FF of 72.3%. Fig. 3(a) shows the J–V characteristics of organic (PDPP3T:$PC_{61}BM$), inorganic (a-Si) and the preferred hybrid tandem solar cell under AM1.5 illumination. The a-Si solar cell has J_{sc} of 9.09 mA cm^{-2}, V_{oc} of 0.83 V, FF of 54.8%, and PCE of 4.15%; the optimized PDPP3T:$PC_{61}BM$ OSCs with a $PF_{EO}SO_3Na$ CIL show J_{sc} of 13.4 mA cm^{-2}, V_{oc} of 0.68 V, FF of 64.6%, and PCE of 5.89%. The PCE of the hybrid tandem solar cells is 7.46%, much higher than that of either of the two cells individually. The *external quantum efficiency* (EQE) of hybrid tandem solar cells is measured under bias light. As shown in Fig. 3(b), the current density of OSC is almost equally distributed in a wide optical cavity (between 650 and 950 nm), which matches the optical window of an a-Si solar cell.

The hybrid tandem solar cell yields a V_{oc} of 1.51 V, which is virtually equal to the sum of the V_{oc} values of the two component cells. In hybrid tandem devices, the ITO/PEDOT:PSS intermediate layer provides a recombinant region for electrons and holes between the top and bottom component cells. Fig. 4 shows the energy-band diagram of a-Si/organic hybrid tandem solar cells, in which the work function of intermediate layer is measured by a scanning Kelvin probe microscope (SKPM). The work function of untreated ITO is 4.70 eV and increases to 4.94 eV after UV–O_3 treatment. The well-matched energy level of treated ITO and PEDOT:PSS may be a reason for the high V_{oc} observed in our hybrid tandem devices.[37]

It will be noticed that the FF of the double-junction device is maintained at the high value of 72.3%. In tandem solar cells, the FF is mainly affected by the current-limiting sub-cell.[16,18] The current density calculated from EQE result shows that the a-Si top-cell has a J_{sc} of 7.49 mA cm^{-2}, which is higher than that of 6.91 mA cm^{-2} for the PDPP3T:$PC_{61}BM$ OSCs (Table 2). We therefore believe that the FF of the organic/a-Si double-junction cell is promoted mainly by the organic bottom-cell. Furthermore, the FF of PDPP3T:$PC_{61}BM$ OSCs shows a notable increase if the incident light is filtered by an a-Si solar cell (Table 1); this implies that PDPP3T:$PC_{61}BM$ OSCs could give a higher FF value as the bottom component cell in an organic/a-Si tandem device than in a single junction device. This leads to a high FF for the hybrid double-junction device.

Table 1 Device performance of single-junction OSCs

OSCs	Back-contact	J_{sc} (mA cm^{-2})	V_{oc} (mV)	FF (%)	PCE (%)
PDPP3T:$PC_{71}BM$	Ca/Al	14.27	660	59.5	5.60
PDPP3T:$PC_{71}BM$ with a-Si filter	Ca/Al	5.64	620	61.5	2.15
PDPP3T:$PC_{61}BM$	Ca/Al	12.27	680	63.5	5.30
PDPP3T:$PC_{61}BM$ with a-Si filter	Ca/Al	5.94	660	67.5	2.65
PDPP3T:$PC_{61}BM$	$PF_{EO}SO_3Na$/Al	13.43	680	64.6	5.89

Table 2 Device performance of hybrid tandem solar cells with different thicknesses of a-Si thin films

a-Si (nm)	V_{oc} (mV)	J_{top} (mA cm^{-2})	J_{bottom} (mA cm^{-2})	J_{tandem} (mA cm^{-2})	FF_{tandem} (%)	PCE_{tandem} (%)
125	1.53 ± 0.03	10.41	6.23	5.29 ± 0.15	72.3 ± 1.4	5.75 ± 0.3
87	1.43 ± 0.05	8.05	6.64	5.94 ± 0.18	72.3 ± 1.6	6.19 ± 0.2
72	1.50 ± 0.01 (1.51)	7.49	6.91	6.50 ± 0.23 (6.73)	72.3 ± 1.1 (73.4)	7.06 ± 0.4 (7.46)

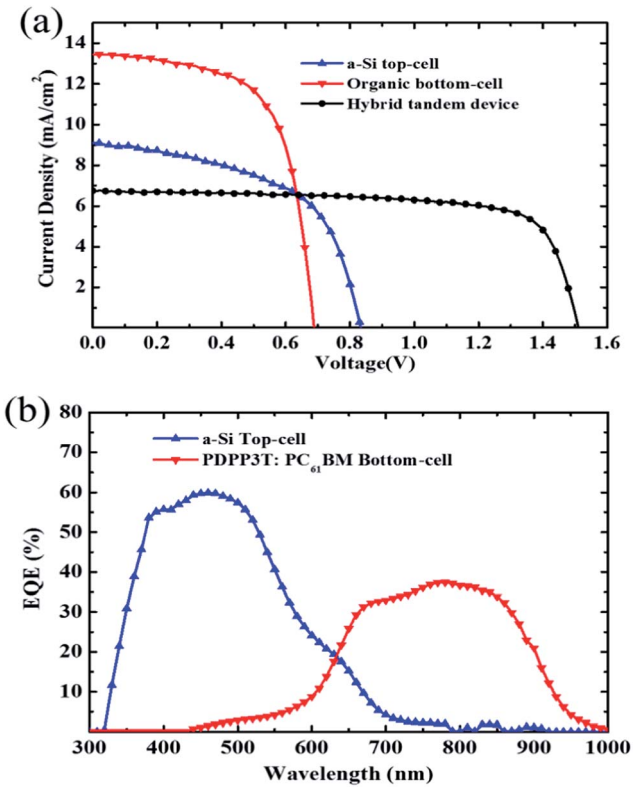

Fig. 3 (a) J–V characteristics of organic (PDPP3T:$PC_{61}BM$), inorganic (a-Si) and the new hybrid tandem solar cell under AM1.5 illumination; (b) EQE spectra of the organic/a-Si hybrid tandem solar cells under different bias lighting.

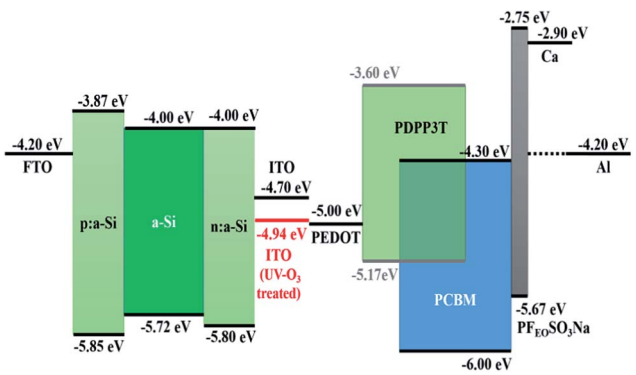

Fig. 4 Approximate energy band diagram of the organic/a-Si hybrid tandem solar cell taken from literature ref. 23 and 26 The work function of the ITO layer was measured by SKPM.

It has been demonstrated that the EQE of single junction OSCs can be as high as 80%,[38–40] and ~8% PCE has been achieved using conjugated polymers with a bandgap of 1.38 eV.[38] It is therefore possible for organic/a-Si tandem solar cells to achieve a J_{sc} of 12.9 mA cm^{-1}, as has been obtained in an a-Si/nc-Si tandem solar cell[41] by further optimization of the a-Si solar cells, the intermediate layers and OSCs. Regarding the measured V_{oc} of 1.51 V and FF of 72.3% in the present study, it is estimated that the PCE of organic/a-Si tandem cells can be improved to ~14%, and this potentially makes the organic/a-Si hybrid tandem cell photovoltaic technology highly efficient.

Conclusions

This study provides an effective cell design for achieving a high efficiency organic/a-Si hybrid tandem device. A high performance organic/a-Si hybrid tandem solar cell has been successfully fabricated using a low bandgap polymer, PDPP3T. The complementary absorption of OSCs and a-Si solar cells extends the spectral range of tandem devices to 950 nm. A high PCE of 7.5% has been obtained for organic/a-Si hybrid tandem solar cells, with V_{oc} of 1.51 V and FF of 72.3%. We have shown that the V_{oc} of organic/a-Si hybrid tandem solar cells almost equals the sum of the sub-cell V_{oc} components under standard AM1.5 illumination, due to a well-matched energy level of the intermediate layer; the FF of 72.3% is the highest value so far achieved for organic/a-Si hybrid tandem solar cells. Further theoretical analysis suggests that organic/a-Si hybrid tandem solar cells with PCE up to 14% should be technically feasible using an optimized low bandgap polymer.

Acknowledgements

This study was financially supported by the National Natural Science Foundation of China under Grant no. 21374120. The authors are grateful for financial support from the Chinese National University Research Fund (GK261001009), Shaanxi Normal University, Xi'an, China, and J. Zhang acknowledges the support provided by the 100 Talents Program of the Chinese Academy of Sciences.

References

1 T. Kinoshita, D. Fujishima, A. Yano, A. Ogane, S. Tohoda, K. Matsuyama, Y. Nakamura, N. Tokuoka, H. Kanno, H. Sakata, M. Taguchi and E. Maruyama, in *Proceedings of 26th European Photovoltaic Solar Energy Conference*, Hamburg, German, 2011, pp. 871–874.

2 H.-P. Wang, T.-Y. Lin, C.-W. Hsu, M.-L. Tsai, C.-H. Huang, W.-R. Wei, M.-Y. Huang, Y.-J. Chien, P.-C. Yang, C.-W. Liu, L.-J. Chou and J.-H. He, *ACS Nano*, 2013, **7**, 9325–9335.
3 H.-P. Wang, T.-Y. Lin, M.-L. Tsai, W.-C. Tu, M.-Y. Huang, C.-W. Liu, Y.-L. Chueh and J.-H. He, *ACS Nano*, 2014, **8**, 2959–2969.
4 W.-R. Wei, M.-L. Tsai, S.-T. Ho, S.-H. Tai, C.-R. Ho, S.-H. Tsai, C.-W. Liu, R.-J. Chung and J.-H. He, *Nano Lett.*, 2013, **13**, 3658–3663.
5 X. Shen, B. Sun, D. Liu and S.-T. Lee, *J. Am. Chem. Soc.*, 2011, **133**, 19408–19415.
6 Y. Zhang, F. Zu, S.-T. Lee, L. Liao, N. Zhao and B. Sun, *Adv. Energy Mater.*, 2014, **4**, DOI: 10.1002/aenm.201300923.
7 W. Shockley and H. J. Queisser, *J. Appl. Phys.*, 1961, **32**, 510–519.
8 L. C. Hirst and N. J. Ekins-Daukes, *Next Generation (Nano) Photonic and Cell Technologies for Solar Energy Conversion*, 2010, vol. 7772, p. 777211.
9 S. Guha, J. Yang, A. Banerjee, T. Glatfelter, K. Hoffman and X. Xu, *Sol. Energy Mater. Sol. Cells*, 1994, **34**, 329–337.
10 L. W. James, R. L. Moon, R. D. Fairman and R. L. Bell, *IEEE Trans. Electron Devices*, 1975, **22**, 1061–1061.
11 S. Guha, *J. Non-Cryst. Solids*, 1996, **198**, 1076–1080.
12 T. Ameri, N. Li and C. J. Brabec, *Energy Environ. Sci.*, 2013, **6**, 2390–2413.
13 Z. H. Hu, X. B. Liao, X. B. Zeng, Y. Y. Xu, S. B. Zhang, H. W. Diao and G. L. Kong, *Acta Phys. Sin.*, 2003, **52**, 217–224.
14 M. A. Green, *Third Generation Photovoltaics: Advanced Solar Energy Conversion*, Springer-Verlag, Berlin, 2003.
15 M. R. Khan, B. Ray and M. A. Alam, *Sol. Energy Mater. Sol. Cells*, 2014, **120**, 716–723.
16 J. Yang and S. Guha, *Appl. Phys. Lett.*, 1992, **61**, 2917–2919.
17 H. Keppner, P. Torres, J. Meier, R. Platz, D. Fischer, U. Kroll, S. Dubail, J. A. A. Selvan, N. P. Vaucher, Y. Ziegler, R. Tscharner, C. Hof, N. Beck, M. Goetz, P. Pernet, M. Goerlitzer, N. Wyrsch, J. Veuille, J. Cuperus, A. Shah and J. Pohl, *Advances in Microcrystalline and Nanocrystalline Semiconductors–1996*, 1997, vol. 452, pp. 865–876.
18 T. Soderstrom, F. J. Haug, V. Terrazzoni-Daudrix and C. Ballif, *J. Appl. Phys.*, 2010, **107**, 014507.
19 J. Steinhauser, J. F. Boucher, E. Omnes, D. Borrello, E. Vallat-Sauvain, G. Monteduro, M. Marmelo, J. B. Orhan, B. Wolf, J. Bailat, S. Benagli, J. Meier and U. Kroll, *Thin Solid Films*, 2011, **520**, 1218–1222.
20 H. Keppner, J. Meier, P. Torres, D. Fischer and A. Shah, *Appl. Phys. A: Mater. Sci. Process.*, 1999, **69**, 169–177.
21 S. Guha, J. Yang and B. J. Yan, *Sol. Energy Mater. Sol. Cells*, 2013, **119**, 1–11.
22 R. E. I. Schropp, H. Li, R. H. J. Franken, J. K. Rath, C. H. M. van der Werf, J. A. Schüttauf and R. L. Stolk, *Sol. Energy Mater. Sol. Cells*, 2009, **93**, 1129–1133.
23 D. Fischer, S. Dubail, J. A. A. Selvan, N. P. Vaucher, R. Platz, C. Hof, U. Kroll, J. Meier, P. Torres, H. Keppner, N. Wyrsch, M. Goetz, A. Shah and K. D. Ufert, *Conference Record of the Twenty Fifth IEEE Photovoltaic Specialists Conference–1996*, 1996, pp. 1053–1056.
24 G. Li, R. Zhu and Y. Yang, *Nat. Photonics*, 2012, **6**, 153–161.
25 F. C. Krebs, *Sol. Energy Mater. Sol. Cells*, 2009, **93**, 394–412.
26 C. J. Brabec, *Sol. Energy Mater. Sol. Cells*, 2004, **83**, 273–292.
27 T. Kim, J. H. Jeon, S. Han, D.-K. Lee, H. Kim, W. Lee and K. Kim, *Appl. Phys. Lett.*, 2011, **98**, 183503.
28 J. Peet, J. Y. Kim, N. E. Coates, W. L. Ma, D. Moses, A. J. Heeger and G. C. Bazan, *Nat. Mater.*, 2007, **6**, 497–500.
29 J. H. Seo, D.-H. Kim, S.-H. Kwon, M. Song, M.-S. Choi, S. Y. Ryu, H. W. Lee, Y. C. Park, J.-D. Kwon, K.-S. Nam, Y. Jeong, J.-W. Kang and C. S. Kim, *Adv. Mater.*, 2012, **24**, 4523–4527.
30 J. Hou, H.-Y. Chen, S. Zhang, R. I. Chen, Y. Yang, Y. Wu and G. Li, *J. Am. Chem. Soc.*, 2009, **131**, 15586–15587.
31 S. Albrecht, B. Grootoonk, S. Neubert, S. Roland, J. Wördenweber, M. Meier, R. Schlatmann, A. Gordijn and D. Neher, *Sol. Energy Mater. Sol. Cells*, 2014, **127**, 157–162.
32 J. C. Bijleveld, A. P. Zoombelt, S. G. J. Mathijssen, M. M. Wienk, M. Turbiez, D. M. de Leeuw and R. A. J. Janssen, *J. Am. Chem. Soc.*, 2009, **131**, 16616–16617.
33 L. Ye, S. Q. Zhang, W. Ma, B. H. Fan, X. Guo, Y. Huang, H. Ade and J. H. Hou, *Adv. Mater.*, 2012, **24**, 6335–6341.
34 T. Shi, X. Zhu, D. Yang, Y. Xie, J. Zhang and G. Tu, *Appl. Phys. Lett.*, 2012, **101**, 161602.
35 Z. He, C. Zhong, S. Su, M. Xu, H. Wu and Y. Cao, *Nat. Photonics*, 2012, **6**, 591–595.
36 Y. Zhou, C. Fuentes-Hernandez, J. Shim, J. Meyer, A. J. Giordano, H. Li, P. Winget, T. Papadopoulos, H. Cheun, J. Kim, M. Fenoll, A. Dindar, W. Haske, E. Najafabadi, T. M. Khan, H. Sojoudi, S. Barlow, S. Graham, J.-L. Brédas, S. R. Marder, A. Kahn and B. Kippelen, *Science*, 2012, **336**, 327–332.
37 Y. Chen, W.-C. Lin, J. Liu and L. Dai, *Nano Lett.*, 2014, **14**, 1467–1471.
38 Z. He, C. Zhong, X. Huang, W.-Y. Wong, H. Wu, L. Chen, S. Su and Y. Cao, *Adv. Mater.*, 2011, **23**, 4636–4643.
39 C. Liu, K. Wang, X. Hu, Y. Yang, C.-H. Hsu, W. Zhang, S. Xiao, X. Gong and Y. Cao, *ACS Appl. Mater. Interfaces*, 2013, **5**, 12163–12167.
40 A. K. K. Kyaw, D. H. Wang, V. Gupta, W. L. Leong, L. Ke, G. C. Bazan and A. J. Heeger, *ACS Nano*, 2013, **7**, 4569–4577.
41 M. A. Green, K. Emery, Y. Hishikawa, W. Warta and E. D. Dunlop, *Prog. Photovoltaics Res. Appl.*, 2014, **22**, 1–9.